Mosaicing Touchless and Mirror-Reflected Fingerprint Images

Heeseung Choi, Kyoungtaek Choi, and Jaihie Kim

***Abstract*—Touchless fingerprint sensing technologies have been explored to solve problems in touch-based sensing techniques because they do not require any contact between a sensor and a finger. While they can solve problems caused by the contact of a finger, other difficulties emerge such as a view difference problem and a limited usable area due to perspective distortion. In order to overcome these difficulties, we propose a new touchless fingerprint sensing device capturing three different views at one time and a method for mosaicing these view-different images. The device is composed of a single camera and two planar mirrors reflecting side views of a finger, and it is an alternative to expensive multiple-camera-based systems. The mosaic method can composite the multiple view images by using the thin plate spline model to expand the usable area of a fingerprint image. In particular, to reduce the affect of perspective distortion, we select the regions in each view by minimizing the ridge interval variations in a final mosaiced image. Results are promising as our experiments show that mosaiced images offer 29% more true minutiae and 28% larger good quality area than one-view, unmosaiced images. Also, when the side-view images are matched to the mosaiced images, it gives more matched minutiae than matching with one-view frontal images. We expect that the proposed method can reduce the view difference problem and increase the usable area of a touchless fingerprint image. Furthermore, the proposed method can be applied to other biometric applications requiring a large template for recognition.**

***Index Terms*—Distance map (DM), image mosaicing, recursive ridge mapping, stitching line, thin plate spline (TPS), touchless fingerprint.**

I. Introduction

FINGERPRINT recognition systems have been widely adopted for user authentication due to their reliable performance and usability compared to other biometric systems. Recently, various kinds of fingerprint image acquisition sensors (including optical, solid-state, thermal, ultrasound, etc.) have been utilized in a wide range of forensic and commercial applications, e.g., criminal investigation, e-commerce, access control, issuing national ID cards and e-passports, etc. Because these types of sensing systems are touch-based, users must press or roll their fingers onto a platen surface to capture fingerprint images. Unfortunately, this capturing scheme often introduces degraded images due to skin deformation (due to skin elasticity and nonuniform pressure), skin condition changes (due to environmental changes and skin characteristics), and latent fingerprints on the sensor surface. Figs. 1(a) and (b) are two different images from the same finger. Due to skin deformation, the relative positions of minutiae sets from the two images are different. Figs. 1(c) and (d) show a minutiae type change due to the nonuniform pressure of the finger. As shown in Fig. 1(e), the ridge-valley contrast of an image can be severely affected by variations in skin condition, and Fig. 1(f) shows that a latent fingerprint remaining on the sensor surface can degrade the enhancement result of a newly captured image. Therefore, representation of the same fingerprint can vary at each acquisition, resulting in the inevitable degradation of the authentication performance [1]. Also, the rise in forgeries in touch-based sensor systems has become a serious problem [29], [30], while some individuals avoid public usage of touch-based sensors due to concerns regarding hygiene [2].

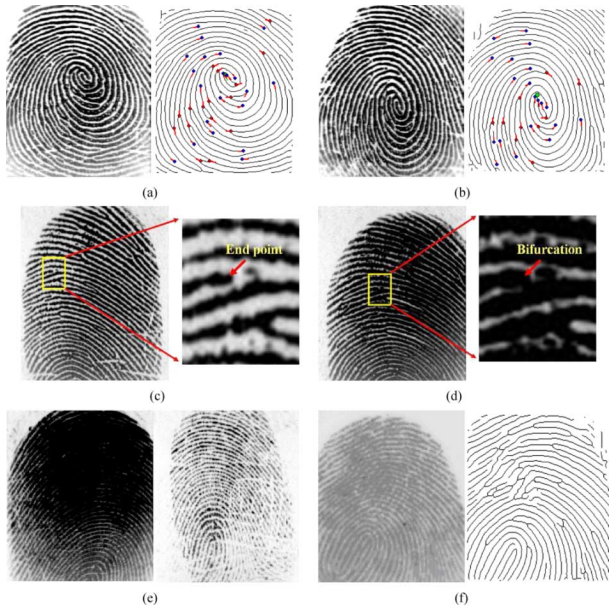

Fig. 1. Distorted images acquired from a touch-based sensor.

To solve the above-mentioned problems, several advances in fingerprint sensing technology have been explored [3]. The multispectral fingerprint imaging (MSI) technique [4] was introduced to acquire better quality images from dry or wet fingers, and optical sensors with high resolution (over 1000 dpi) have been proposed to observe finer fingerprint features including sweat pores, incipient ridges, scars, and so on [5], [6]. However, these techniques are also touch-based, so they are not free from

Manuscript received August 10, 2009; accepted November 17, 2009. First published January 12, 2010; current version published February 12, 2010. This work was supported by the Korea Science and Engineering Foundation (KOSEF) through the Biometrics Engineering Research Center at Yonsei University [R112002105070010(2009)]. The associate editor coordinating the review of this manuscript and approving it for publication was Prof. Davide Maltoni.

The authors are with Biometric Engineering Research Center, Yonsei University, Seoul 120-749, Korea (e-mail: mcnas@yonsei.ac.kr; maninquestion@yonsei.ac.kr; jhkim@yonsei.ac.kr).

Color versions of one or more of the figures in this paper are available online at http://ieeexplore.ieee.org.

Digital Object Identifier 10.1109/TIFS.2009.2038758

the problems caused by nonuniform, inconsistent, and irreproducible contacts.

To overcome these kinds of problems, a touchless fingerprint sensing technology has been proposed that does not require any contact between a sensor and a finger. Thus, the finger's minutiae and ridge information cannot be changed or distorted as it will be free of skin deformation. Also, it can capture fingerprint images consistently because it is not affected by different skin conditions or latent fingerprints. Recently, several companies and research groups have developed touchless fingerprint sensors and recognition systems [7]–[9]. TST Group developed a touchless imaging sensor (BiRD III) which uses a complementary metal–organic–semiconductor (CMOS) camera, and red and green light sources to acquire fingerprint images [7]. Song *et al.* [8] proposed a sensing system with a single charged-coupled device (CCD) camera and double ring-type blue illuminators to capture high contrast images. Also, Mitsubishi Electric Corporation proposed another touchless approach transmitting the light through the finger [9], acquiring fingerprint patterns under the surface of skin using light with a wavelength of 660 nm. However, such sensing systems [7]–[9] have an inherent problem as they use only a single capturing device, such as CMOS or CCD cameras. As shown in Fig. 2(a), when capturing an image using a single camera, the geometrical resolution of the fingerprint image decreases from the fingerprint center towards the side area [1]. Therefore, false features may be obtained in the side area and it reduces the valid and useful region for authentication. Moreover, if there is a view difference between images due to finger rolling [see Fig. 2(b)], it reduces the common area between fingerprints and degrades system performance. To solve this problem, 3-D touchless sensing systems using more than one view have been explored [10]–[13]. TBS [10] used five cameras placed around a finger to capture nail-to-nail fingerprint images and generated a 3-D fingerprint image using the *shape-from-silhouette* method. They then unwrapped the 3-D finger image onto a 2-D image by using parametric and nonparametric models to make rolled-equivalent images [11]. Fatehpuria *et al.* [12] proposed a 3-D touchless device using multiple cameras and structured light illumination (SLI). The structured light patterns are projected onto a finger to obtain its 3-D shape information and 2-D unfolded images are generated by applying "*Springs algorithm*" and some postprocessing steps. Also, the Hand Shot ID system was developed to acquire a 3-D shape of a hand with fingers by stitching images from 36 cameras [13]. Although all these methods attempted to solve the problems in touch-based sensors and acquire expanded fingerprint images with less skin deformation, they did not raise much interest in the market because of much higher costs compared to conventional touch-based sensors.

Considering the above observations, we adopt a new touchless sensing scheme using a single camera and a set of mirrors. The mirrors work as virtual cameras, thus enabling the capture of an expanded view of a fingerprint at one time without using multiple cameras. This general concept was already suggested in [11]. However, even though the authors mentioned the principle possibility of the method, they did not provide any implementation examples and practical applications. In this paper, we explain how to design the device in detail and provide an image mosaic method to acquire a complete extended fingerprint image. The device consists of a single camera, two planar mirrors, light-emitting diode (LED)-based illuminators, and a lens. Two planar mirrors are used to reflect the left and right side view of a finger. To acquire the expanded fingerprint image, we also propose a new mosaic method to combine frontal- and side-view images. We consider minutiae and ridge points as the correspondences for initial alignment, and use the thin plate spline (TPS) model and ridge mapping for finer alignment. In particular, to reduce ridge width variation caused by perspective distortion and to preserve the ridge intervals of a mosaiced image as consistently as possible, we select the regions to be mosaiced from three views by comparing the ridge width values in all images. The rest of this paper is organized as follows: in Section II, brief descriptions of the proposed device are given. In Section III, the proposed mosaic method is presented. Experimental results are shown in Section IV, and conclusions and future works are drawn in Section V.

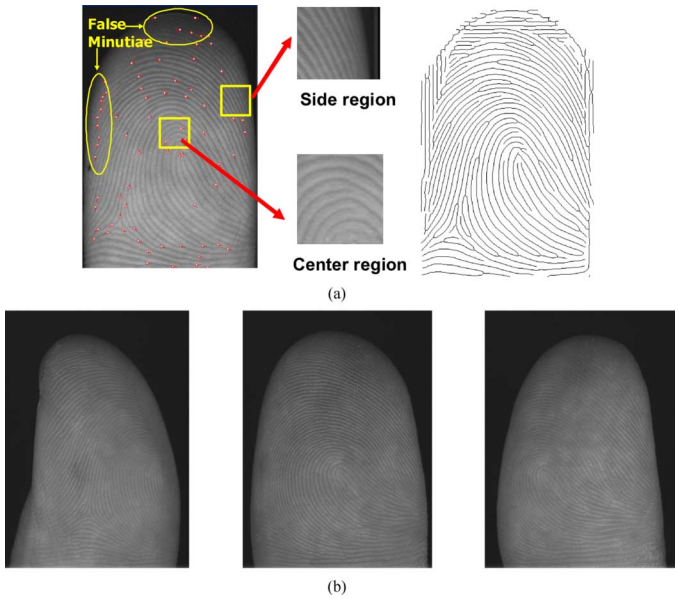

Fig. 2. Difficulties in touchless fingerprint recognition. (a) False minutiae extraction due to the geometrical resolution difference between center and side regions. (b) View difference problem due to finger rolling.

II. System Design

To overcome the view difference problem and the limitation of a single view, some touchless fingerprinting systems capture several different views of a finger by using multiple cameras. However, using multiple cameras increases the cost and size of a system. Thus, we adopt a new sensing system which captures three different views (frontal, right, and left) at one time by using a single camera and two planar mirrors. Figs. 3(a) and (b) show the prototype and schematic view of the device. As shown in Fig. 3, two mirrors are placed next to the finger and reflect the right and left side views of the finger. Then, the frontal view and two mirror-reflected views are captured by a single camera simultaneously. A mirror-reflected image is regarded as the "flipped" image taken by a virtual camera placed at a different direction compared to the real one [14]. Therefore, we can capture three different views of a fingerprint using only one

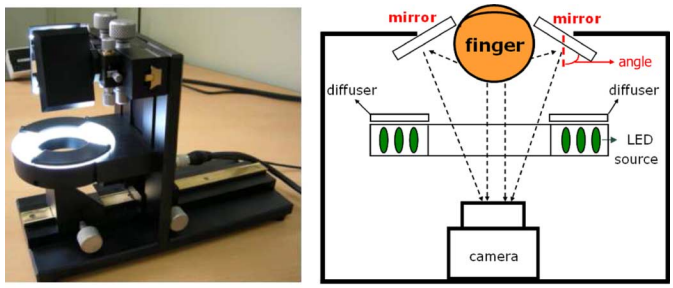

Fig. 3. Proposed device. (a) Prototype of the device. (b) Schematic view of the device.

camera and also avoid the synchronization problem existing in multiple camera-based systems.

In addition, to obtain high-quality fingerprint images, we need to consider several optical components in order to design the device. The specifications of the optical components are as follows:

1) Camera and lens: We use a 1/3-in progressive scan type CCD with 1024×768 active pixels, where the pixel size is 4.65×4.65 μm. This camera offers a sufficient frame rate of 29 Hz, thus avoiding image blurring caused by typical finger motion [31]. Also, we use simple equations [see (1) and (2)] to design an adequate lens for our system [33]

$$M = \frac{q}{p} \tag{1}$$

$$\frac{1}{f} = \frac{1}{p} + \frac{1}{q} \tag{2}$$

where f is the lens focal length, p and q are the lens-to-object and lens-to-image distances, respectively, and M is the optical magnification. Normally, the required image resolution for touch-based sensors is 500 dpi. Therefore, to ensure a 500-dpi spatial resolution in the fingerprint area and to cover three view fingerprints, the optical magnification parameter M, the lens to image distance q, and field of view (FOV) are determined as 0.1, 170 mm, and 50×38 mm, respectively. By doing this, we can capture three view images with 500-dpi resolution at one time. Also, the depth of field (DOF) of the lens ranges from -2.6 to $+2.6$ mm at a given working distance and it normally covers the half depth of a finger.

2) Illumination: Considering the reflectance of human skin to various light sources [16], we used ring-shaped white LED illuminators and a bandpass filter which can transmit green light to enhance the ridge-to-valley contrast. Also, the illuminators are placed perpendicular to the finger to remove the shadowing effect [1]. Diffusers are used to illuminate a finger uniformly.

3) Mirror: Two planar mirrors are positioned next to the left and right side of the finger and the mirror size is determined to cover the maximum thumb size [15]. To provide enough overlapping area between frontal- and side-view images, the angles of the mirrors [see Fig. 3(b)] are determined 15° empirically. Also, the mirrors can be used as pegs to place a user's finger firmly on the device.

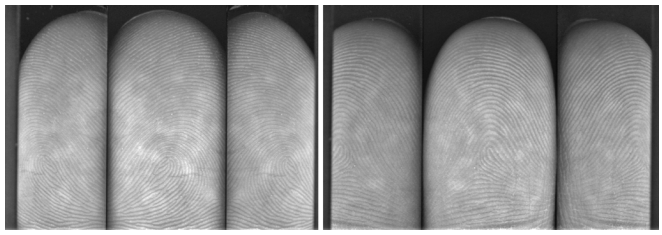

Fig. 4. Examples of captured images from the device.

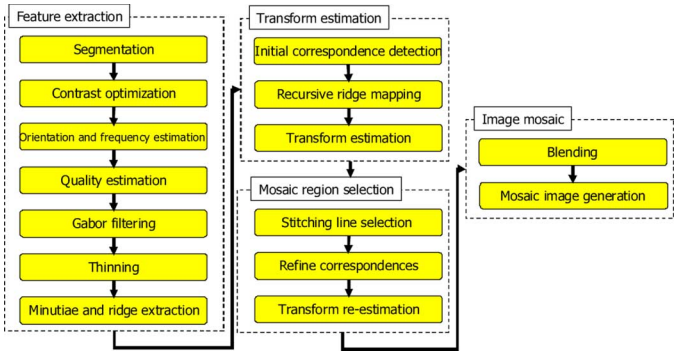

Fig. 5. Overall flowchart of the proposed mosaicing method.

The images captured by the proposed device are shown in Fig. 4. As shown in this figure, we can capture the frontal, left, and right side fingerprint image at one time.

III. Proposed Mosaic Method

In this section, we explain the mosaic method for synthesizing an expanded fingerprint image from frontal- and side-view images. The overall scheme of the method is presented in Fig. 5. The method is mainly composed of four stages (feature extraction, transform estimation, mosaic region selection and final mosaic). In feature extraction, we extract minutiae and ridge information of each fingerprint and detect correspondences using minutiae and ridge points. After that, we estimate the transform for aligning the center and side image, and mosaic regions on the three images are selected to expand the effective area of a fingerprint image. Finally, these three different view images are combined to generate a mosaiced image through the blending procedure. In the rest of this section, we explain the proposed mosaic method in detail.

A. Feature Extraction

Before estimating the transform between frontal- and side-view images, it is necessary to find the correspondences between the images. We use the minutiae and ridges as corresponding features because they are distinctive and easily localized for representing a fingerprint. To find the minutiae and ridges, we apply some preprocessing steps as follows:

1) Segmentation: After acquiring the three view images (frontal, left side, and right side), we divide each image into 8×8 pixel blocks. Then, the mean and variance of gray values of each block are calculated to determine the foreground (fingerprint) and background regions in the images.

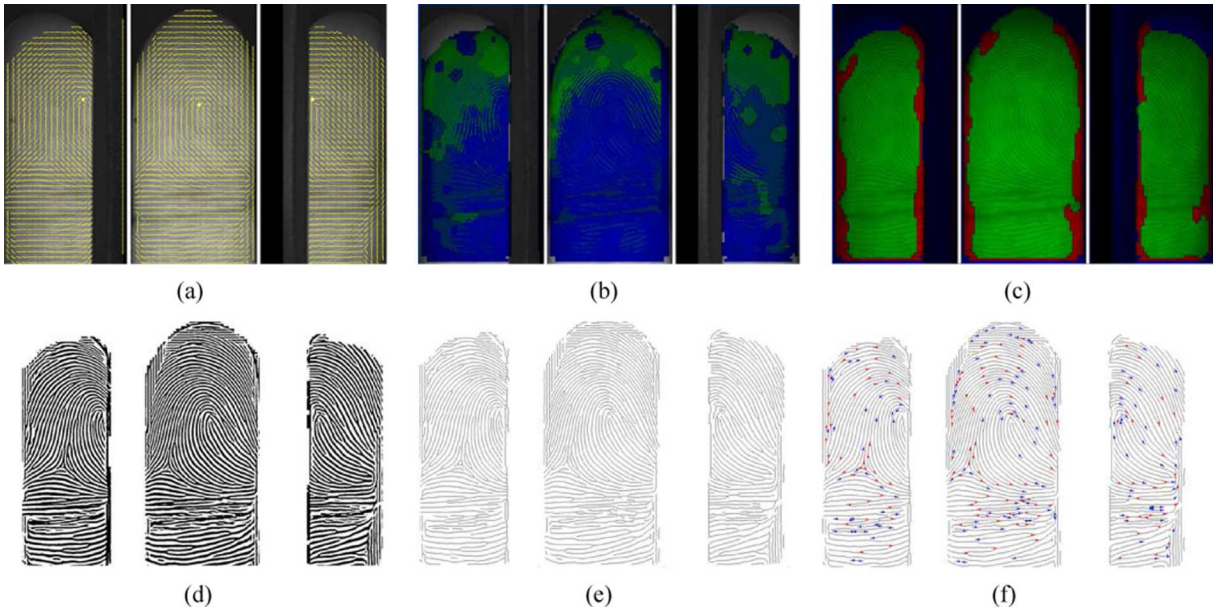

Fig. 6. Preprocessing steps. (a) Orientation estimation. (b) Frequency estimation. (c) Quality estimation. (d) Gabor filtering. (e) Thinning. (f) Minutiae and ridge extraction.

2) Contrast optimization: The contrast of the touchless images may not be sufficient to process directly. Therefore, block histogram equalization and normalization [17] are applied to enhance the contrast of the images.
3) Orientation and ridge frequency estimation: We apply the regression method [18] to estimate ridge orientation [see Fig. 6(a)], and the local ridge frequency is calculated by using the method [32] which models the local ridge pattern as a sinusoidal-shaped surface [see Fig. 6(b)].
4) Ridge and minutiae extraction: A bank of Gabor filters is applied to extract the ridges. The filter bank parameters are adjusted to cover possible ranges of the ridge frequency for 16 directional orientations. To preserve the ridge information in the fingerprint boundary region as much as possible, we apply the Gabor filter with frequency-adaptive standard deviation [8]. Then, binarized and thinned image is obtained as shown in Fig. 6(e) and (f).
5) Quality estimation: To obtain the true ridge and minutia sets, the quality of the image should be measured. We adopt the method referred in [19] to estimate the quality of the image [see Fig. 6(c)], and use only the minutia and ridge information obtained from good quality regions to remove the negative influence of false ridges and minutiae when mosaicing three views.

B. Transform Estimation

1) Initial Correspondence: Before estimating the transform to align the side-view image to the frontal-view image, correspondences between them should be established. Two side mirrors can be considered as virtual cameras, so we can apply the epipolar constraint to detect the correspondences. To apply the constraint easily, we use image rectification [33]. The process creates a configuration where the set of epipolar lines corresponding to a set of matched minutiae is transformed into a set of horizontal lines. Thus, it simplifies the matching process since scanning is only needed along the horizontal direction

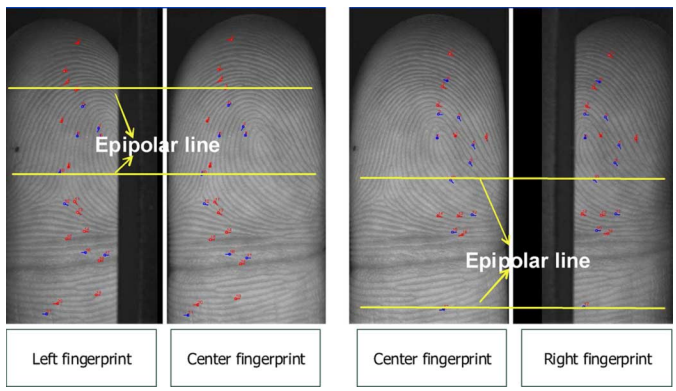

Fig. 7. Examples of the initial matched minutiae in the images.

with small bounds when matching the minutiae. The rectification process uses the calibration parameters computed in the camera calibration phase when the system is installed. Therefore, the precalculated transform parameters can be used every time when images are newly captured. After that, we first match the minutiae, and then the ridge points attached to the matched minutiae are matched gradually to increase the correspondences between the images. To eliminate the false minutiae matches, we use the graph matching method [20] observing the geometrical relationship among the minutiae. Examples of matched minutiae between two images are shown in Fig. 7. In the figure, we can see that matched minutiae are on the same horizontal lines due to image rectification. Then, the sampled ridge points are matched using the dynamic programming (DP) method [21], and the ridge points are sampled at every eighth pixel on each ridge curve.

2) Transform Estimation: After initial correspondences are determined, we estimate the transform to align frontal and side images. The relation between frontal and mirror-reflected views cannot be modeled as a linear transformation (e.g., homography) because a finger is not a planar surface and the cameras

(one real and two virtual) are related by rotation and translation. Therefore, in this paper, we use a nonlinear transform model called the TPS, and adopt our earlier work [21] to estimate the transform using the correspondences. The entire procedure for the transform estimation is summarized as follows.

a) Detect the correspondences (matched minutiae and ridge points attached to them).

b) Estimate the initial TPS transformation f by minimizing the energy function $E_{\mathrm{TPS}}(f)$ as shown in (3)

$$E_{\mathrm{TPS}}(f) = \sum_{a=1}^{K} \|y_a - f(v_a)\|^2 + \lambda \int \left[\left(\frac{\partial^2 f}{\partial x^2} \right)^2 + 2 \left(\frac{\partial^2 f}{\partial x \partial y} \right)^2 + \left(\frac{\partial^2 f}{\partial y^2} \right)^2 \right] dxdy \quad (3)$$

where y_a and v_a represent the correspondence in each image. Also, the matrix form of (3) can be described as follows:

$$E_{\mathrm{TPS}}(d, \omega) = \|Y - Vd - \Phi\omega\|^2 + \lambda \mathrm{trace}(\omega^T \Phi \omega) \quad (4)$$

where V and Y are $K \times 3$ matrices whose rows are the K correspondences in homogeneous coordinates, and Φ represents a symmetric matrix whose (i, j) element value is $\|v_j - v_i\|^2 \log \|v_j - v_i\|$. And after QR decomposition, the least square solutions of parameter d and ω are calculated.

c) Calculate the registration error E_R when frontal and side images are aligned by the initially estimated transform. The registration error E_R can be calculated as follows:

$$E_R = (1 - w_1)(\mathrm{RME}_F + \mathrm{RME}_S) + w_1(E_c^F + E_c^S), \quad 0 < w_1 < 1 \quad (5)$$

where $\mathrm{RME}_F(\mathrm{RME}_S)$ indicates how well the ridges of the frontal (side) image is aligned to the corresponding ridges of the side (frontal) image. The weight parameter w_1 is set to 0.2 empirically. And to measure the RME_F and RME_S quantitatively, we use the distance map (DM) [24]. The DM is the image composed of the values defined as the minimum distance from a given point to the nearest ridge in the thinned image. We also normalize the distance values of the image (see Fig. 8) to handle the variation of the ridge interval between the frontal and side images

$$D(x, y) = \frac{D_r(x, y)}{(D_r(x, y) + D_v(x, y))} \quad (6)$$

where $D_r(x, y)$ and $D_v(x, y)$ represent the distances from a given point (x, y) to the nearest ridge and valley, respectively. Therefore, the ridge mapping error (RME) values are easily measured as follows:

$$\mathrm{RME}(r_i) = \frac{1}{N_i} \sum_{n=1}^{N_i} D(f(\vec{x_n})) \quad (7)$$

where N_i represents the number of ridge points at the ridge r_i in the frontal (side) image, and $\vec{x_n}$ is a point on ridge r_i and $D(f(\vec{x_n}))$ is the distance value at the corresponding position of $\vec{x_n}$ on the DM of the side (frontal) image.

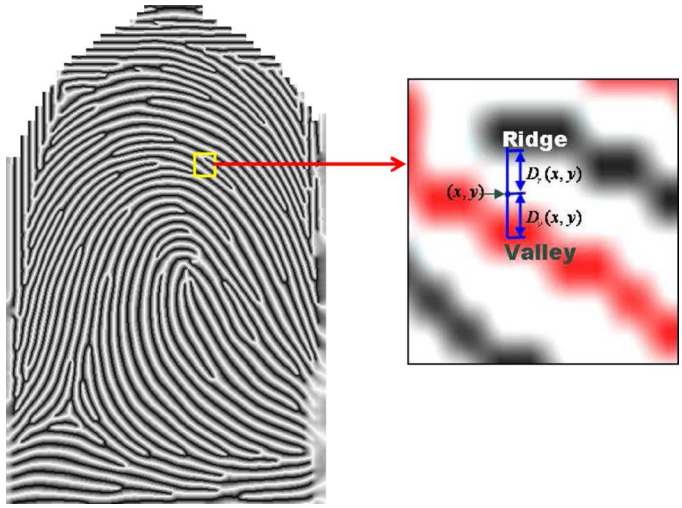

Fig. 8. Normalized DM of a fingerprint image.

Also, $E_c^F(E_c^S)$ represents the inverse consistency error of the transformation from the frontal (side) image to the side (frontal) image [21], [34]. The inverse consistency error deals with the error between the original points and the points obtained by inverse-transformation of the transformed points. It can be calculated as follows:

$$E_C(r_i) = \frac{1}{N_i} \sum_{n=1}^{N_i} \left\| \vec{x_n} - f^{-1}(f(\vec{x_n})) \right\| \quad (8)$$

where N_i represents the number of ridge points at the ridge r_i in the image. $f(\cdot)$ and $f^{-1}(\cdot)$ represent the transformation and the inverse of the transformation, respectively. Therefore, it represents the error caused by ambiguous correspondences between the forward and inverse transformations.

d) To estimate the transformation more accurately, recursive ridge mapping [21] is used to find more corresponding ridge points and eliminate erroneous ridge correspondences. This procedure is repeated and the transform is updated until the registration error E_R dose not decrease anymore or is below a predetermined threshold. Fig. 9 shows the ridge mapping results for transform estimation. As shown in this figure, we use these correspondences to estimate the transformation between frontal- and side-view images.

C. Mosaic Region Selection

In this section, we describe how to select the optimal regions from frontal and side images to generate a mosaic image. Once we have aligned the left and right side images to the frontal image using the estimated transform, we need to decide how to produce the final mosaic image. It mainly consists of two steps: a mosaic region selection and synthesizing a final image. The first step involves a region selection which chooses the regions from each image to contribute to the final composite image. The second step is the synthesizing of a final image with these selected regions while preserving the ridge and valley structures of the fingerprint and minimizing visible seams and blurring. In

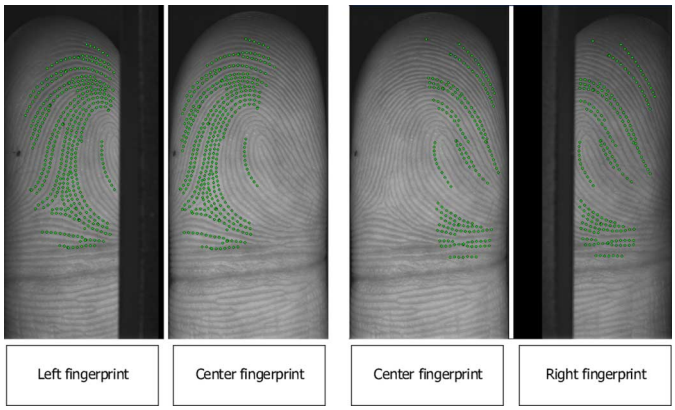

Fig. 9. Ridge mapping result for transform estimation.

Fig. 10. Examples of rolled fingerprint images.

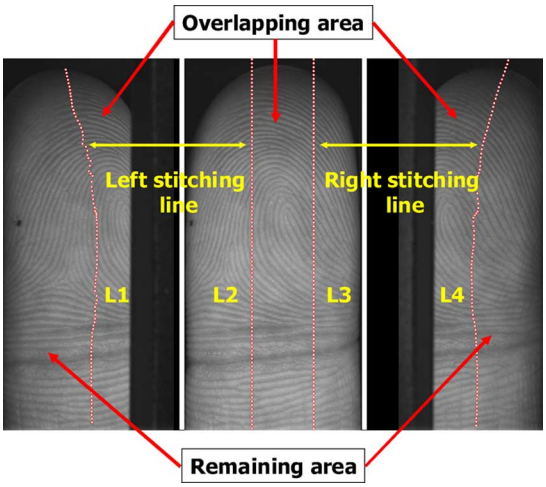

Fig. 11. Mosaic region selection in each image.

our observations, we conclude that a successful touchless fingerprint mosaic method should not only create a smooth transition within the overlapped region between the frontal and side fingerprint, but should also preserve the ridge and valley structures as in a good quality rolled image. As shown in Fig. 10, if finger rolling is well controlled, a fingerprint impression has the characteristic that the ridge and valley orientations are smoothly changed from the center to the side area and the ridge intervals are almost consistent in the whole fingerprint area. However, in our case, three images are captured with different view directions (front, right side, and left side) since we use mirrors as virtual cameras at each side position. Accordingly, in the frontal image, the ridge intervals decrease from the center area to the side area of the fingerprint. On the other hand, in the side images, the ridge intervals decrease from the side area to the center area of the fingerprint (see Fig. 4). Therefore, we must choose the center region in the frontal image and the side region in the left and right images properly to ensure consistent ridge intervals when the final mosaiced image is generated. Also, we must find the regions in each image having almost the same ridge intervals. Fortunately, estimating the ridge intervals in each image is simple since we already calculated the DM of the image as discussed in Section III-B. By using the precalculated DM, we obtain the two stitching lines in the center image as the boundaries of the participating region for the final mosaic image. Each stitching line corresponds to the boundary curve of the participating region in a side image for combining with the frontal region. We divide the DM of each image into 8×8 pixel blocks, and the maximum value in each block $D_B(\cdot)$ is computed and considered as a ridge interval in the block

$$D_B(\vec{x}) = \max_{\Delta\vec{x} \in W} (D(\vec{x} + \Delta\vec{x})) \tag{9}$$

where W is an 8×8 window and $\Delta\vec{x}$ is a vector within a block. $D(\vec{x})$ is the distance value at $\vec{x}$ position in the DM. By using the method described in the above section, we already calculate the transform f from frontal to side images. Thus, we find a vertical stitching line L in the frontal image by minimizing the following equation:

$$\min_{L} \sum_{\vec{x} \in L} \|D_{B\_F}(\vec{x}) - D_{B\_S}(f(\vec{x}))\| \tag{10}$$

where L represents the vertical line of the frontal image, $D_{B\_F}(\vec{x})$ and $D_{B\_S}(\vec{x})$ are the block DMs of the frontal and side image which have the ridge interval information in each block. As a result, we can select the left ($L2$) and the right ($L3$) stitching lines in the frontal images and their corresponding curves ($L1$ and $L4$) in the side images as shown in Fig. 11. Then we decide the overlapping area as the inside region between the left and right stitching line ($L2$, $L3$) in the frontal image. The remaining areas (the left side of $L1$, the right side of $L4$) are selected to composite the left and right area of the mosaic image. The correspondences selection process is then applied to recalculate the transform for the final mosaic. The TPS kernel $\phi(r) = r^2 \log r$ is a log function depending on the distance from the control points (correspondences). Accordingly, as the distance increases, the influence of the nonrigid term decreases rapidly. Therefore, the points far from the control points are transformed by an affine transform rather than a nonrigid transform. By using the control points only in the overlapping area as shown in Fig. 12, the remaining region is warped slightly relative to the overlapping region. Therefore, the remaining regions are not heavily deformed and have a tendency to preserve their original ridge and valley structures as before.

D. Image Mosaic

To generate the final mosaiced image, we still need to blend the images to eliminate the visible artifact edges in the seam between the center and side images, due to intensity differences and geometrical misalignments. In the stitching regions, enough ridge and valley structure should be retained since blurring or misalignment in these regions may generate false features or

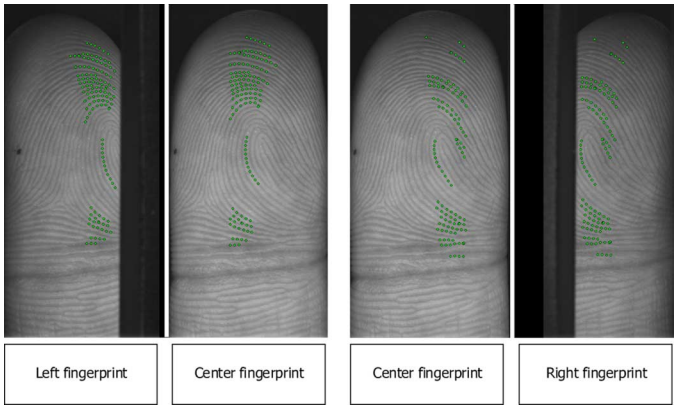

Fig. 12. Final correspondences for transform recalculation.

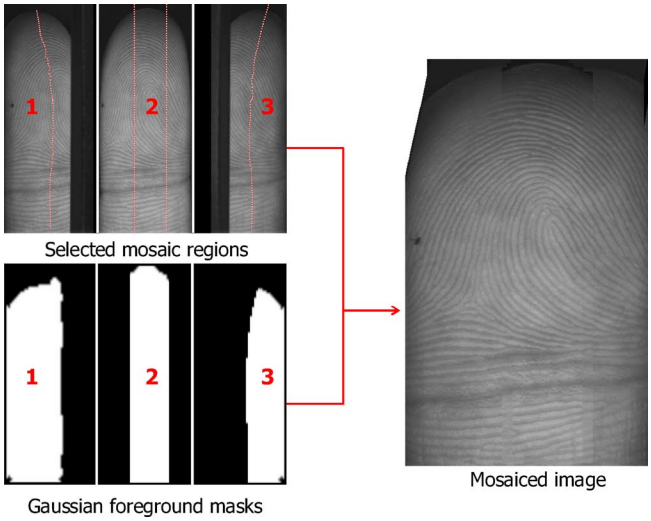

Fig. 13. Gaussian foreground mask generation and final mosaiced image.

miss true features in the final image. Therefore, we use the modified center method to blend the images [21], [26]. In this method, the mosaiced image is a weighted combination of the input images and the weighting coefficients which vary spatially as a function of the distance from the foreground of each image.

For implementation, the foreground masks of the frontal and side images which have zero values in background areas in each image are generated first. They are convolved with a 19×19 Gaussian filter G and pixel values in the mosaic image $I_M(\vec{x})$ are assigned to the weighted sum of frontal and side images ($I_F(\vec{x})$ and $I_S(\vec{x})$)

$$w(\vec{x}) = G * M(\vec{x}) \tag{11}$$

$$\begin{cases} \text{If } w_F(\vec{x}) = 1, \;\; I_M(\vec{x}) = I_F(\vec{x}) \\ \text{else if } w_S(\vec{x}) = 1, \;\; I_M(\vec{x}) = I_S(\vec{x}) \\ \text{else } I_M(\vec{x}) = \frac{I_F(\vec{x}) \times w_F(\vec{x}) + I_S(f(\vec{x})) \times w_S(f(\vec{x}))}{w_F(\vec{x}) + w_S(f(\vec{x}))} \end{cases} \tag{12}$$

where M denotes the foreground mask of a given image and $w(\vec{x})$ is the weight of the position $\vec{x}$. The weights are inversely proportional to the distance from the positions to each foreground region with a weight of 1. And then we compensate the global intensity difference between the images by smoothing the intensity values in the transition area. Fig. 13 shows the Gaussian masks generated from the three images and the final blending results. As shown in the figure, the ridge structures in the mosaiced image are well preserved and the ridge width is made smooth in the stitched region. Fig. 14 shows the comparison between the frontal and mosaiced image from the same subject. As shown in the figure, we can see that our mosaic method expands the usable region in the frontal image while preserving ridge and valley structures in the side regions, and ridge and minutiae are extracted as well after some preprocessing steps.

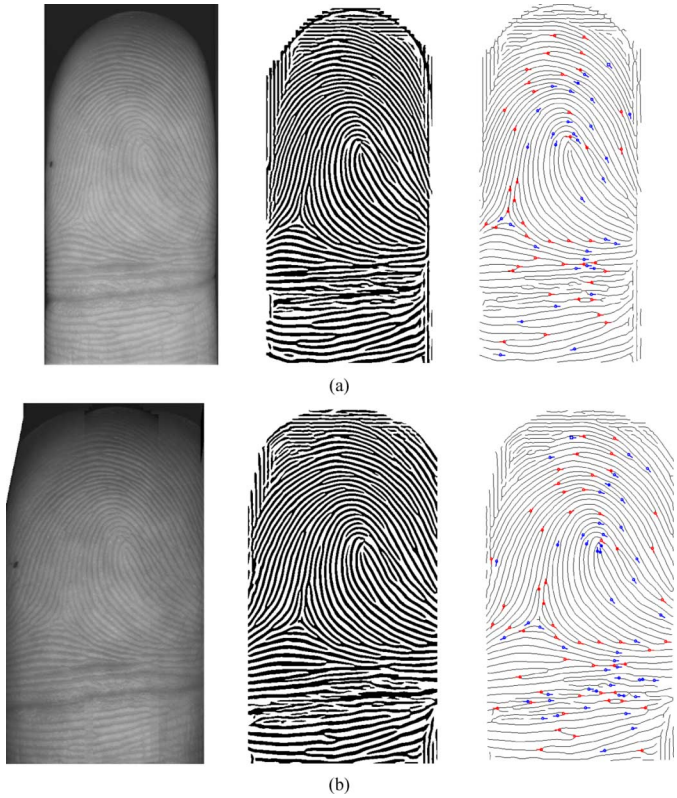

Fig. 14. Enhanced mosaiced images for recognition. (a) Frontal image and its enhanced image. (b) Mosaiced image and its enhanced image.

IV. Experimental Results

For the experiments, we collected fingerprint images from 112 different fingers (corresponding to 112 different subjects). For each subject, the frontal, left, and right view images are captured using the device, and then 112 mosaiced images were generated via the proposed method. Some mosaic results and their processed images are shown in Fig. 15. As shown in the figure, our method produces expanded images having consistent ridge and valley intervals in the side areas. To verify the usefulness of the proposed method quantitatively, we compared the frontal images and their mosaiced images in three aspects: the increasing rate of true minutiae, the increasing rate of foreground fingerprint size, and the number of matched minutiae with side-view images.

As discussed in [25]–[27], the most definite indicator of mosaiced image quality is the number of true minutiae additionally extracted. Therefore, five experts working on fingerprint recognition manually selected true minutiae in both frontal and mosaiced images. As shown in Fig. 16, the number of true minutiae increased for all subjects with the average increase of 29.53%.

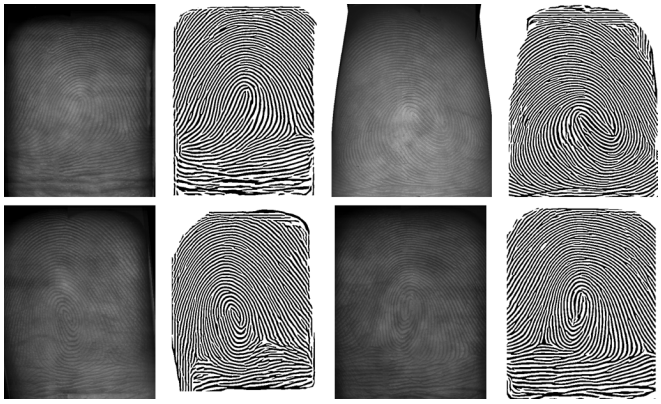

Fig. 15. Examples of mosaiced and enhanced images.

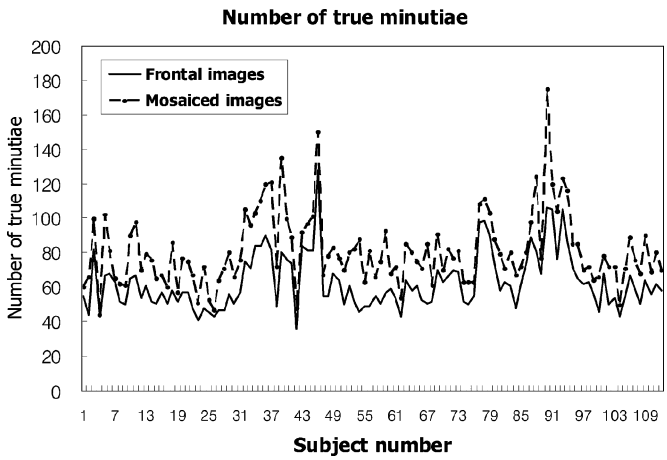

Fig. 16. Comparisons of the number of true minutiae in frontal and mosaiced images.

In some fingerprints, there were a few minutiae in the side area. As a consequence, only very small numbers of minutiae were additionally obtained when mosaicing was performed. However, in general, our mosaic results provided a greater number of true minutiae than the original frontal images. Also, when we captured the corresponding fingerprint images using a conventional 500 dpi optical sensors with 280×320 pixels (the IZZIX FD1000 from Digent Co. Ltd), the number of true minutiae was around 40. However, when using our device, the number of true minutiae of frontal images was around 60. Based on this comparison, we can maintain that our touchless sensor is sufficiently competitive since the sensor can obtain more minutiae information than conventional frustrated total internal reflection (FTIR)-based sensors.

To inspect the increase of the usable area for fingerprint recognition, we applied three fingerprint quality checking methods to compare the foreground size of both frontal and mosaiced images. Here, foreground means the good quality regions of a fingerprint which have true minutiae and ridges. As mentioned in Section I, the side area of a one-view touchless image may not have enough quality for recognition because the ridge and valley structures are indistinguishable in the area. We used the three fingerprint quality checking methods (standard deviation [17], coherence [28], and gradient-based method [19]) to measure the increased number of good quality blocks in mosaiced images. Even though each measurement is used for touch-based fingerprint quality estimation, they can extract the quality values in each local block by measuring the clarity and consistency of ridge and valley structures. For fair comparisons, equal threshold value was applied to both frontal and mosaic images. We then calculated the number of good quality blocks in both images. Table I shows the increasing rates of foreground size based on each quality measurement. The results show that the foreground size of a mosaiced image increases more than 28% in all cases. This means that our mosaiced images have enough clarity between the ridge and valley in the side areas. Therefore, it will provide more true information than just a one-view image. And, Fig. 17 shows the fingerprint quality representation in both frontal and mosaiced image. For easy comprehension, good and bad quality regions are represented as green and red area, respectively. As shown in the figure, good quality regions increased in mosaiced image when we applied the same threshold value. Based on the above two comparisons, we can see that the mosaiced images contain more useful information than the original frontal images. However, one of the main problems in touchless recognition is the matching problem when a view-difference image is captured due to the rolling of a finger. Therefore, we performed the matching between the frontal- and side-view (left and right) images of each individual. Also, the same matching procedure was applied to the mosaiced and side-view images. Unfortunately, there was no matching method optimized for our touchless images, so we applied the touch-based minutiae matching in [20] to calculate the number of matched minutiae in each case. The method considers the overall minutiae information including minutiae position, orientation and types (end point or bifurcation) and

TABLE I
AVERAGE INCREASING RATE OF FOREGROUND SIZE IN TERMS OF EACH MEASUREMENT

Quality measurement	Average increasing rate of foreground size
Standard deviation [17]	28.65%
Coherence [28]	33.72%
Gradient-based method [19]	30.81%

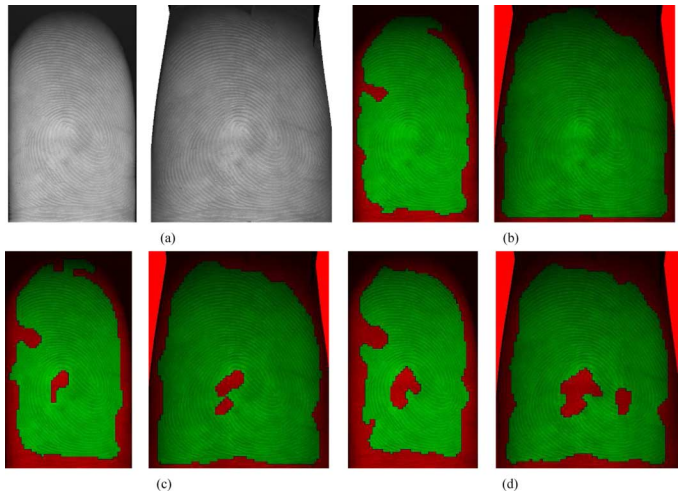

Fig. 17. Fingerprint quality representation. (a) Frontal and mosaiced image. (b) Quality representation when using Standard deviation method [17]. (c) Quality representation when using Coherence method [28]. (d) Quality representation when using Gradient-based method [19].

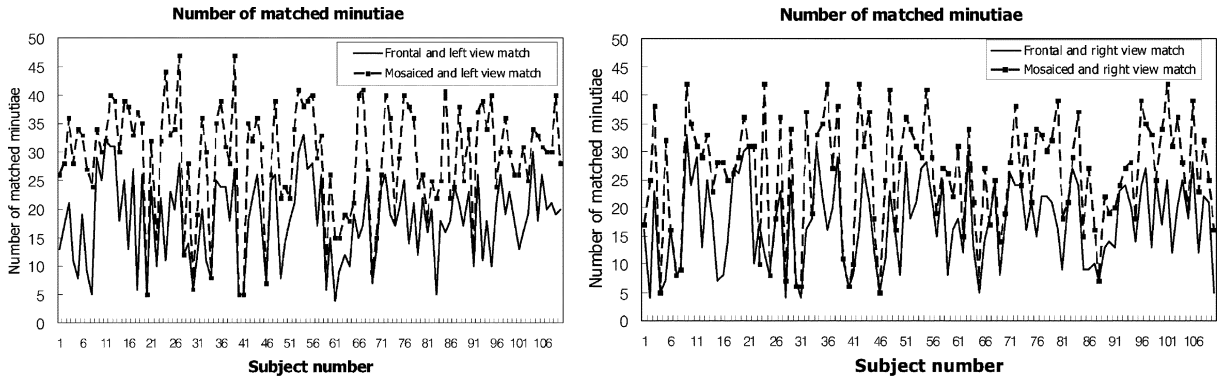

Fig. 18. Comparison of the number of matched minutiae.

can be used as one of the performance measurements to analyze the similarity between the side and mosaiced fingerprints. As shown in Fig. 18(a) and (b), the number of matched minutiae increased in most images of both (left and right view match) cases. This means our method can composite the image without the large amount of deformation in the side area. In some cases, the number of matched minutiae did not increase because of the lack of minutiae in the side regions. However, we can expect that our mosaiced images can enhance the performance when view difference images are matched.

V. Conclusions and Future Work

This paper describes a novel touchless fingerprint sensing device which covers three views of a fingerprint and a method for mosaicing these images to expand the effective area of a fingerprint. The device is composed of a single camera and two flat mirrors and it offers an alternative to an expensive multiple-camera-based system. In addition, we used a TPS model to calculate the transform between frontal- and side-view images. To calculate the transform more accurately, we used recursive ridge mapping to increase the true correspondences. Based on the observation of good quality rolled images, the ridge and valley intervals of each image are considered in order to select the stitching lines and mosaic regions. The ridge and valley intervals are acquired using the DM and the transform is then refined to preserve the ridge structures and ridge width of a final image. Our mosaic results are promising in terms of increasing the true minutiae rate, increasing the foreground size rate and the number of matched minutiae. On average, the number of true minutiae increased by 29.53%, and the foreground size increasing rate was calculated using the three quality measurement. Consequently, the rates are above 28% in all quality measurements. To verify the usefulness of the mosaic method, the side-view images are matched to both frontal and mosaiced images. The results showed that the mosaiced images have more matched minutiae than the frontal images when side-view images are sensed. Therefore, using the mosaiced images, we can solve the view difference problems in recognition and also generate a large template. According to the results, we expect that the proposed method can be adopted in other vision-based fingerprint applications. And when we compare our mosaic image and corresponding touch-based rolled image, the overall ridge structures are very similar and there are small Euclidean distance differences between the corresponding minutiae. When we directly use the minutiae matcher [20], there are many matched minutiae (see Fig. 19). Therefore, we can expect that if we use more optimized matcher, the matching performance can be enhanced further and the compatibility between touchless images and rolled images can be ensured; therefore, it is one of our on-going research projects in touchless fingerprint recognition. Also there are still new challenges. Our method used minutiae as the initial correspondences. Therefore, if matched minutiae are wrongly detected, the mosaic results can be worse due to the misalignment of ridge and valley structures. Therefore, in our future work, we will develop a touchless fingerprint enhancement technique for stable feature extraction. And there was no matching method optimized for touchless images, so it needs to be provided in a near future. Therefore, we will develop the matching method incorporating some invariant features against perspective distortion (such as ridge count). Also touchless images ensure consistent ridge patterns. So if we measure the similarity of overall ridge patterns, then our mosaic results will be better evaluated. Even though our results are well worth enough for the alternative to the legacy rolled images, our mosaic results are not perfectly rolled equivalent images yet compared to the images in [11]. The reason is that we do not make an exact 3-D model of a finger. For making a ground truth rolled fingerprint image, we are going on the research generating 3-D model of a finger using the images acquired from our cost-effective device and developing the method for accurate unwrapping.

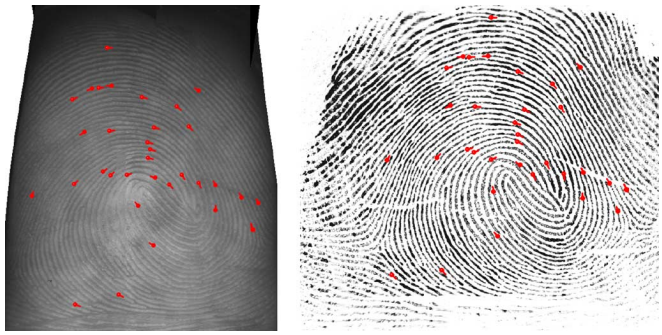

Fig. 19. Matched minutiae between a mosaiced image and corresponding rolled image.

REFERENCES

[1] N. K. Ratha and V. Govindaraju, *Advances in Biometrics: Sensors, Algorithms and Systems*. New York: Springer, 2008.

[2] C. R. Blomeke, S. J. Elliott, and T. M. Walter, "Bacterial survivability and transferability on biometric devices," in *41th IEEE Int. Carnahan Conf. Security Technology*, 2007, pp. 80–84.

[3] S. C. Dass and A. K. Jain, "Fingerprint-based recognition," *Technometrics*, vol. 49, no. 3, pp. 262–276, 2007.

[4] R. K. Rowe, S. P. Corcoran, S. P. Nixon, and R. E. Ostrom, "Multispectral imaging for Biometrics," in *Proc. SPIE Conf. Biometric Technology for Human Identification*, 2005, pp. 90–99.

[5] Cross Match Livesan Systems Aug. 03, 2009 [Online]. Available: http://www.crossmatch.com

[6] A. K. Jain, Y. Chen, and M. Demirkus, "Pores and ridges: High-resolution fingerprint matching using level 3 features," *IEEE Trans. Pattern Anal. Mach. Intell.*, vol. 29, no. 1, pp. 15–27, Jan. 2007.

[7] TST Group Aug. 03, 2009 [Online]. Available: http://www.tst-biometrics.com

[8] Y. Song, C. Lee, and J. Kim, "A new scheme for touchless fingerprint recognition system," in *Proc. Int. Symp. Intelligent Signal Processing and Communication Systems*, 2004, pp. 524–527.

[9] Mitsubishi Touchless Fingerprint Sensor Aug. 03, 2009 [Online]. Available: http://global.mitsubishielectric.com

[10] TBS Touchless Fingerprint Imaging Aug. 03, 2009 [Online]. Available: http://www.tbsinc.com/

[11] Y. Chen, G. Parziale, E. Diaz-Santana, and A. K. Jain, "3D touchless fingerprints: Compatibility with legacy rolled images," in *Proc. Biometric Consortium Conf.*, Baltimore, MD, 2006.

[12] A. Fatehpuria, D. L. Lau, and L. G. Hassebrook, "Acquiring a 2-D rolled equivalent fingerprint image from a non-contact 3-D finger," in *SPIE Defense and Security Symp. Biometric Technology for Human Identification III*, Orlando, FL, 2006, vol. 6202, pp. 62020C-1–62020C-8.

[13] Aug. 03, 2009 [Online]. Available: http://privacy.cs.cmu.edu/dataprivacy/projects/handshot /index.html

[14] I. Lin, J. Yeh, and M. Ouhyoung, "Realistic 3-D facial animation parameters from mirror-reflected multi-view video," in *Proc. Computer Animation 2001, IEEE Computer Society*, Seoul, Korea, Nov. 2001, pp. 2–11.

[15] T. M. Greiner, Hand Anthropometry of U.S. Army Personnel Army Natick Research Development and Engineering Center, Tech. Rep. Natick/TR-92/011, Dec. 1991.

[16] A. Elli, "Understanding the color of human skin," in *Proc. 6th SPIE Conf. Human Vision and Electronic Imaging, SPIE*, May 2001, vol. 4299, pp. 243–251.

[17] L. Hong, Y. Wan, and A. K. Jain, "Fingerprint image enhancement: Algorithm and performance evaluation," *IEEE Trans. Pattern Anal. Mach. Intell.*, vol. 20, no. 8, pp. 777–789, Aug. 1998.

[18] C. Lee, S. Lee, J. Kim, and S. Kim, "Preprocessing of a fingerprint image captured with a mobile camera," in *Proc. IAPR Intl. Conf. Biometrics, ICB, Springer*, Hong Kong, Jan. 2006, vol. 3832, LNCS, pp. 348–355.

[19] S. Lee, H. Choi, and J. Kim, "Fingerprint quality index using gradient components," *IEEE Trans. Inf. Forensics Security*, vol. 3, no. 4, pp. 792–800, Dec. 2008.

[20] D. Lee, K. Choi, and J. Kim, "A robust fingerprint matching algorithm using local alignment," in *Proc. 16th Int. Conf. Pattern Recognition*, 2002, vol. 3, pp. 803–806.

[21] K. Choi, H. Choi, S. Lee, and J. Kim, "Fingerprint image mosaicking by recursive ridge mapping," *Special Issue on Recent Advances in Biometrics Systems, IEEE Trans. Syst., Man, Cybern. B*, vol. 37, no. 5, pp. 1191–1203, Oct. 2007.

[22] A. Ross, S. C. Dass, and A. K. Jain, "Fingerprint warping using ridge curve correspondences," *IEEE Trans. Pattern Anal. Mach. Intell.*, vol. 28, no. 1, pp. 19–30, Jan. 2006.

[23] H. Chui and A. Rangarajan, "A new point matching algorithm for nonrigid registration," *Comput. Vision Image Understanding*, vol. 89, no. 2-3, pp. 114–141, 2003.

[24] D. Lee, K. Choi, S. Lee, and J. Kim, "Fingerprint fusion based on minutiae and ridge for enrollment," in *Proc. 4th Int. Conf. Audio- and Video-based Biometric Person Authentication (AVBPA)*, 2003, pp. 478–485.

[25] N. K. Ratha, J. H. Conell, and R. M. Bolle, "Image mosaicing for rolled fingerprint construction," in *Proc. 4th Int. Conf. Pattern Recognition*, 1998, vol. 2, pp. 1651–1653, 8.

[26] A. K. Jain and A. Ross, "Fingerprint mosaicking," in *Proc. Int. Conf. Acoustic Speech and Signal Processing (ICASSP)*, 2002, vol. 4, pp. 4064–4067.

[27] J. Zhou, D. He, G. Rong, and Z. Bian, "Effective algorithm for rolled fingerprint construction," *Electron. Lett.*, vol. 37, no. 8, pp. 492–494, 2001.

[28] E. Lim, X. Jiang, and W. Yau, "Fingerprint quality and validity analysis," in *IEEE Int. Conf. Image Processing (ICIP)*, Sep. 2002, vol. 1, pp. 469–472.

[29] T. Putte and J. Keuning, "Biometrical fingerprint recognition: Don't get your fingers burned," in *Proc. 4th Working Conf. Smart Card Res. Advanced Appl.*, 2000, pp. 289–303.

[30] T. Matsumoto, H. Matsumoto, K. Yamada, and S. Hoshino, "Impact of artificial gummy fingers on fingerprint systems," in *Proc. SPIE, Optical Security and Counterfeit Deterrence Techniques IV*, 2002, vol. 4677, pp. 275–289.

[31] C. Lee, S. Lee, and J. Kim, "A study of touchless fingerprint recognition system," *Structural, Syntactic, and Statistical Pattern Recognition (LNCS)*, vol. 4109, pp. 358–365, 2006.

[32] D. Maio and D. Maltoni, "Ridge-line density estimation in digital images," in *Proc. 14th Int. Conf. Pattern Recognition*, 1998, vol. 1, pp. 534–538.

[33] A. Fusiello and L. Irsara, "Quasi-Euclidean uncalibrated epipolar rectification," in *Proc. 19th Int. Conf. Pattern Recognition (ICPR)*, Tampa, FL, 2008, pp. 1–4.

[34] H. J. Johnson and G. E. Christensen, "Consistent landmark and intensity-base image registration," *IEEE Trans. Med. Imag.*, vol. 21, no. 5, pp. 450–461, May 2002.

Heeseung Choi received the B.S. and M.S. degrees in electrical and electronic engineering from Yonsei University, Seoul, Korea, in 2004 and 2006, respectively. He is currently pursuing the Ph.D. degree in electrical and electronic engineering from Yonsei University, Seoul, Korea.

He has been a research member of Biometrics Engineering Research Center (BERC). His research interests include computer vision, biometrics, image processing, and pattern recognition.

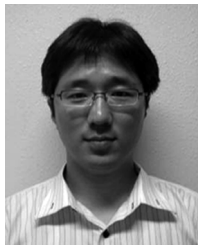

Kyoungtaek Choi received the B.S. degree in electrical and electronics engineering from Chung-ang University, Seoul, Korea, in 2001, and the M.S. and Ph.D. degrees in electrical and electronic engineering from Yonsei University, Seoul, Korea, in 2003 and 2008, respectively.

Currently, he has been researching about fingerprint registration, touchless fingerprint recognition, and fake fingerprint detection. His research interests include computer vision, biometrics, image processing, and pattern recognition.

Jaihie Kim received the B.S. degree in electronic engineering from Yonsei University, Seoul, Korea, in 1979, and the M.S. degree in data structures and the Ph.D. degree in artificial intelligence from Case Western Reserve University, Cleveland, OH, in 1982 and 1984, respectively.

Since 1984, he has been a professor in the School of Electrical and Electronic Engineering, Yonsei University. He is currently the Director of the Biometric Engineering Research Center in Korea. His research areas include biometrics, computer vision, and pattern recognition.

Prof. Kim is currently the Chairman of Korean Biometric Association.